RSC Advances

PAPER

View Article Online
View Journal | View Issue

Cite this: *RSC Adv.*, 2019, **9**, 33625

Enhancing the Vickers hardness, melting point and thermodynamic properties of hafnium dodecaboride†

Yong Pan,*[a] Shuang Chen[a] and Yanlin Jia*[bc]

Received 23rd September 2019
Accepted 14th October 2019

DOI: 10.1039/c9ra07702b

rsc.li/rsc-advances

Although HfB_{12} is a promising surperhard material because of the boron cuboctahedron cage, the Vickers hardness of HfB_{12} remains controversial. We apply first-principles calculations to investigate the influence of a transition metal on the structural stability, Vickers hardness and thermodynamic properties of HfB_{12}. The Vickers hardness of HfB_{12} is 39.3 GPa. In particular, the Vickers hardness of TM-doped HfB_{12}, which are novel superhard materials, is larger than 40 GPa. The Vickers hardness of Re-doped HfB_{12} is up to 47.6 GPa. The improvement of Vickers hardness is that the introduction of an alloying element improves the localized hybridization between B and Hf, and then enhances the bond strength of the B–B covalent bond and the Hf–B bond. In addition, these alloying elements enhance the melting-point and Debye temperature of the HfB_{12}. Therefore, we believe that alloying is an effective method to improve the Vickers hardness and thermodynamic properties of HfB_{12} superhard material.

1. Introduction

Compared to diamond and boron nitride superhard materials, transition metal borides (TMBs) are attractive superhard materials because of their fascinating mechanical, electronic and thermodynamic properties *etc.*[1–9] However, hardness is a complex phenomenon, which is related to the structural configuration, chemical bonding, electronic structure, deformation, defects, *etc.*[10–14] For TMBs superhard materials, previous work has shown that the Vickers hardness is determined by the network and shorter B–B covalent bonds.[15,16] Namely, the boron concentration plays a crucial role in hardness. Therefore, research has focused on the boron-rich borides such as TMB_3, TMB_4 and TMB_{12} in recent years.[17–21] However, the investigation of boron-rich boride faces two key problems: one is that the boron-rich boride has difficulty meeting stable conditions. For example, the published TMB_{12} mainly focuses on the ZrB_{12} and HfB_{12}.[22] The investigation of other TMB_{12} is scarce. Another important factor is that the Vickers hardness of TMBs is also influenced by the TM–B bond, in addition to the B–B covalent bond.

Thus, alloying is an effective approach to improve the bond strength of TM–B bond and then enhance the Vickers hardness of TMBs superhard material.[23–26] For example, Kaner *et al.* work has shown that the measured Vickers hardness of WB_4 with alloyed 20 at% Ti, 10 at% Zr and 6 at% Hf is up to 50.9 ± 2.2 GPa, 55.9 ± 2.7 GPa and 51.6 ± 2.8 GPa, respectively.[27] The WB is not a superhard material. However, Ta addition markedly improves the Vickers hardness of WB, while the measured Vickers hardness of $W_{0.5}Ta_{0.5}B$ is up to 42.8 GPa.[28] Similarly, the Y and Sc additions enhance Vickers hardness of ZrB_{12}, while the measured Vickers hardness of $Zr_{0.5}Y_{0.5}B_{12}$ and $Zr_{0.5}Sc_{0.5}B_{12}$ is up to 45.8 GPa and 48.0 GPa,[29] respectively. Based on the design principle, we believe that the alloying is to improve the bonding state (TM–B bond) and Vickers hardness of TMBs superhard materials.

Among these TMBs, HfB_{12} with cubic structure ($Fm\bar{3}m$) is an attractive superhard material because this dodecaboride is composed of the boron cuboctahedron cage (24 B atoms).[30,31] The boron cage can enhance the Vickers hardness and elastic modulus of HfB_{12}. However, the superhard characteristic of HfB_{12} remains controversy. For example, the recent work has shown that the calculated Vickers hardness of HfB_{12} is 39.1 GPa,[32] which is not a superhard material (≥40 GPa). Therefore, the great challenge of TMBs superhard material is how to enhance the Vickers hardness of HfB_{12}. On the other hand, the thermodynamic properties must be considered as the important factor because the thermal stability plays a crucial role in industrial applications. For instance, diamond does not cut the ferrous material because of the formation of iron when the temperature is above than 600 °C.[33] As a result, an important

[a]*School of Materials Science and Engineering, Southwest Petroleum University, Chengdu, 610500, China. E-mail: y_pan@ipm.com.cn*

[b]*College of Materials Science and Engineering, Central South University, Changsha, 410083, China. E-mail: jiayanlin@126.com*

[c]*College of Materials Science and Engineering, Beijing University of Technology, 100 Ping Le Yuan, Chaoyang District, Beijing 100124, China*

† Electronic supplementary information (ESI) available. See DOI: 10.1039/c9ra07702b

work is how to improve the melting point and Debye temperature of superhard materials.

In the present work, we apply the first-principles approach to investigate the influence of alloying elements on the Vickers hardness, elastic modulus and thermodynamic properties of HfB_{12}. We consider five possible transition metals: Nb(4d-), Mo(4d-), W(5d-), Re(5d-) and Os(5d-), respectively. Our work shows that these alloying elements not only enhance the Vickers hardness, but also improve the melting point and Debye temperature of HfB_{12}. Therefore, we predict that TM-doped HfB_{12} is a novel superhard material.

2. Theoretical methods

To explore the TMBs superhard materials, we mainly focus on the boron-rich TMBs. Therefore, HfB_{12} with the cubic structure is likely to a potential superhard material. The experimental lattice parameter of HfB_{12} is $a = 7.377$ Å. HfB_{12} with a unit-cell has 52 atoms, which are composed of B cuboctahedron cage. The structural configuration of HfB_{12} is shown in ESI.† It is obvious that the network B–B covalent bond is the origin of high hardness of HfB_{12}. However, the Vickers hardness of HfB_{12} is also affected by the bond strength of Hf–B bond, in addition to the network B–B covalent bonds. To improve the bond strength of Hf–B bond and enhance the Vickers hardness, one Hf atom in a unit-cell is replaced by the 4d- and 5d-transition metal.

In this paper, the Vickers hardness of HfB_{12} with alloying elements is calculated by the semiempirical model.[34] On the other hand, the Vickers hardness of a solid is indirectly estimated by the elastic modulus and brittle behavior. Here, the elastic constants of TM-doped HfB_{12} are calculated by the stress *vs.* stain method.[35,36] The elastic modulus of TM-doped HfB_{12} is obtained by the elastic constants. Here, we consider three elastic parameters: bulk modulus, shear modulus and Young modulus,[37–41] respectively. The bulk modulus and shear modulus of TM-doped HfB_{12} are calculated by the Voigt–Reuss–Hill (VRH) approximation.[42,43] In addition, the Vickers hardness of TMBs is indirectly demonstrated by the B/G ratio.[44,45] The general trend is, the lower the B/G ratio, the high Vickers hardness for the TMBs.[46,47]

In addition, we should be considered the thermodynamic stability of alloying elements in HfB_{12}. Here, the thermodynamic stability of TM-doped HfB_{12} is estimated by the impurity formation energy (E_f),[48] which is given by:

$$\Delta E_f = E_{HfB_{12}}^{Hf\rightarrow TM} - E_{HfB_{12}} + \mu_{Hf} - \mu_{TM} \quad (1)$$

where $E_{HfB_{12}}^{Hf\rightarrow TM}$ and $E_{HfB_{12}}$ are the total energy of TM-doped HfB_{12} and the HfB_{12}, respectively. μ_{Hf} and μ_{TM} are the chemical potential of Hf and TM (TM = Nb, Mo, W, Re and Os) elements. The chemical potential of a solid is estimated by the electronic energy difference. When considering the elemental phases, the chemical potential is simply proportional to the Gibbs energy of the system.[49,50]

About thermodynamic properties, we consider two important parameters: the melting point and Debye temperature, respectively. The melting point of TM-doped HfB_{12} is calculated by:[51,52]

$$T_m = 354 + 4.5(2C_{11} + C_{33})/3 \quad (2)$$

The Debye temperature of TM-doped HfB_{12} is calculated by the average sound velocity, which is obtained by:[53,54]

$$\theta_D = \frac{h}{k_B}\left(\frac{3n}{4\pi\Omega}\right)^{1/3} \times v_m \quad (3)$$

where h and n are the Planck constant and the number of atoms in a unit-cell, respectively. The average sound velocity (v_m) in a system is given by:

$$v_m = \left[\frac{1}{3}\left(\frac{2}{v_t^3} + \frac{1}{v_l^3}\right)\right]^{-1/3} \quad (4)$$

where v_t and v_l are the transverse elastic wave velocity and longitudinal elastic wave velocity, which are given by:

$$v_t = \left(\frac{G}{\rho}\right)^{1/2} \quad (5)$$

$$v_l = \left(\frac{3B + 4G}{3\rho}\right)^{1/2} \quad (6)$$

All calculations in this paper were calculated by the first-principles calculations, as implemented in the CASTEP code.[55,56] The exchange-correlation-function was treated by the generalized gradient correction(GGA) within Perdew–Burke–Ernzerhof functional (PBE) functional.[57,58] The cutoff energy of HfB_{12} with alloying element was 400 eV for the plane-wave expansion. The integration in the Brillouin zone was carried out by the k-point grid of $5 \times 5 \times 5$. The interaction between the ionic and valence electron was treated by the ultrasoft pseudopotential.[59,60] The SCF tolerance was smaller than 1.0×10^{-6} eV/atom and the maximal displacement was lower than 0.001 Å. During the process of structural optimization, all systems were relaxed.[61–63]

3. Results and discussions

To investigate the influence of alloying elements on the Vickers hardness of HfB_{12}, Fig. 1 shows the calculated Vickers hardness of TM-doped HfB_{12}, and the HfB_{12} for comparison. It can be seen that the calculated Vickers hardness of HfB_{12} is 39.3 GPa, which is in good agreement with the Korozlu *et al.* work (39.1 GPa).[64] When TM atom is introduced, it is found that these alloying elements markedly enhance the Vickers hardness of HfB_{12}. In particular, the calculated Vickers hardness of Re-doped HfB_{12} is up to 47.6 GPa, which is 21.1% larger than that of the HfB_{12}. It must be mentioned that the calculated Vickers hardness of TM-doped HfB_{12} is above 40 GPa, indicating that TM-doped HfB_{12} are novel superhard materials. Therefore, we believe that alloying is an effective method to enhance the Vickers hardness of TMBs.

To demonstrate the influence of transition metal on the hardness of HfB_{12}, Fig. 2 shows the calculated bulk modulus, shear modulus and Young's modulus of TM-doped HfB_{12} and the HfB_{12}. Here, the calculated bulk modulus, shear modulus

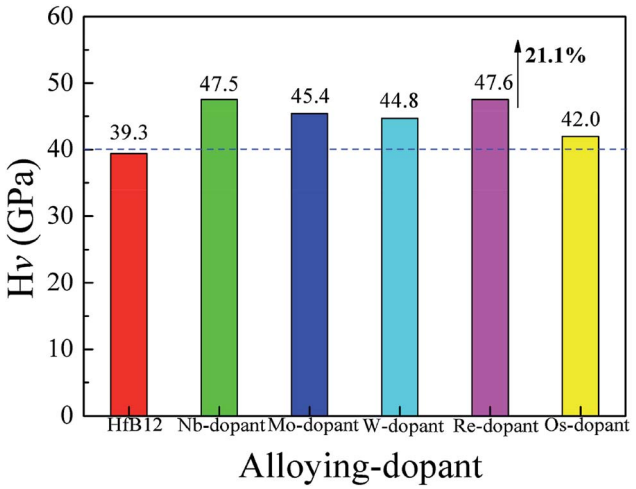

Fig. 1 Calculated Vickers hardness of TM-doped HfB_{12} and the parent HfB_{12}.

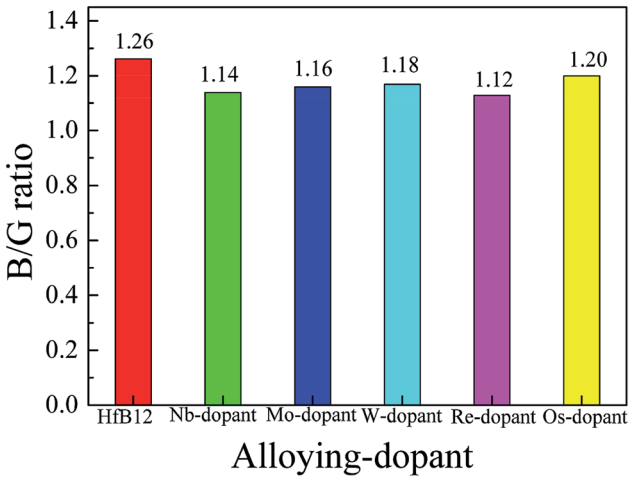

Fig. 3 Calculated B/G ratio of TM-doped HfB_{12} and the parent HfB_{12}.

and Young's modulus of HfB_{12} are 238.2 GPa, 188.6 GPa and 447.6 GPa, respectively, which are in good agreement with the other theoretical results.[64] When Hf atom is substituted by the TM atom, although the calculated bulk modulus of TM-doped HfB_{12} is smaller than that of the HfB_{12}, the calculated shear modulus and Young's modulus of TM-doped HfB_{12} are larger than that of the HfB_{12}. As mentioned above, it is concluded that these alloying elements enhance the shear deformation resistance and elastic stiffness of the HfB_{12}. Here, the calculated shear modulus and Young's modulus of Nb-doped HfB_{12} are 210.0 GPa and 487.3 GPa, respectively, which are larger than that of the other TM-doped HfB_{12}. Namely, the 4d-Nb enhances the shear deformation resistance and elastic stiffness of HfB_{12} in comparison to 5d-TM. The increasing of shear deformation is that these alloying elements improve the localized hybridization between B and Hf along the shear direction. This result is demonstrated by the variation of chemical bonding (see charge density distribution).

As mentioned above, we know that the Vickers hardness of TMBs is indirectly demonstrated by the B/G ratio. To demonstrate the variation of hardness, Fig. 3 displays the calculated B/G ratio of TM-doped HfB_{12} and the HfB_{12}. The calculated B/G ratio of the HfB_{12} is 1.26, indicating that HfB_{12} is a brittle material. Note that the calculated B/G ratio of TM-doped HfB_{12} is smaller than that of the HfB_{12}. This result indicates that these alloying additions enhance the Vickers hardness of the HfB_{12}. The trend of B/G ratio is consistent with the variation of Vickers hardness of TM-doped HfB_{12}.

Based on the analysis of mechanical properties, we believe that these alloying elements enhance the Vickers hardness of the HfB_{12}. Following, it is necessary to study the stability of alloying elements in HfB_{12}. Table 1 lists the calculated lattice parameter, density, volume and impurity formation energy of

Table 1 Calculated lattice parameters (Å), density, ρ (g cm^{-1-3}), volume, V ($Å^3$) and impurity formation energy E_f (kJ mol^{-1}) of HfB_{12} with alloying elements, and the HfB_{12}

Element	Method	a	ρ	V	E_f
HfB_{12}	Cal	7.389	5.07	403.4	
	Exp[64]	7.377			
	Theo[65]	7.312			
Nb-dopant		7.376	4.75	401.3	−16.63
Mo-dopant		7.373	4.76	400.8	−13.85
W-dopant		7.369	5.14	400.2	−13.28
Re-dopant		7.373	5.14	400.7	−11.08
Os-dopant		7.382	5.14	402.3	−7.46

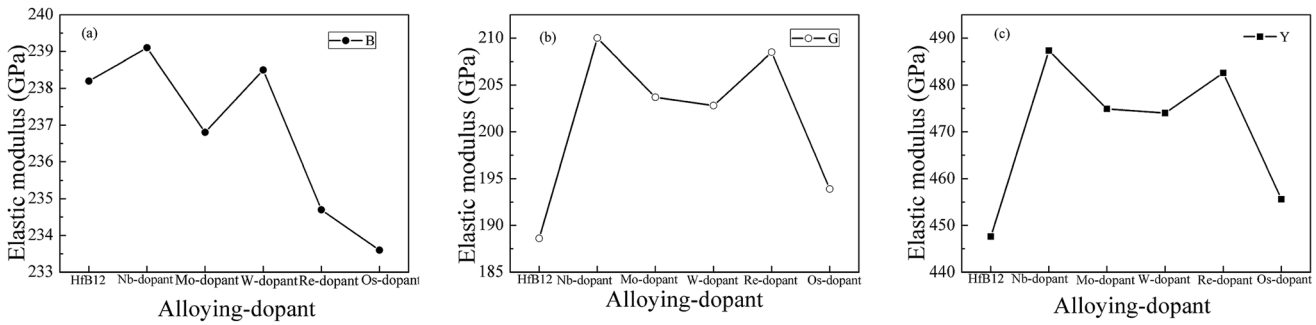

Fig. 2 Calculated elastic modulus of TM-doped HfB_{12} and the HfB_{12}, (a) bulk modulus, (b) shear modulus and (c) Young's modulus, respectively.

TM-doped HfB_{12}. It is found that these alloying elements are thermodynamic stability in HfB_{12} because the calculated impurity formation energy of TM-doped HfB_{12} is smaller than zero. It is worth noticing that the calculated impurity formation energy of TM-doped HfB_{12} increases gradually with increasing the atomic number. This trend may be related to the valence electronic configuration of TM atom. Here, the thermodynamic stability of TM-doped HfB_{12} follows the order of Nb-dopant > Mo-dopant > W-dopant > Re-dopant > Os-dopant.

Naturally, the trend of thermodynamic stability is related to the electronic interaction between atoms, which are demonstrated by the variation of lattice parameter. As listed in Table 1, firstly, we find that the calculated lattice parameter of the HfB_{12} is $a = 7.389$ Å, which is in good agreement with the other theoretical result and experimental data.[64,65] However, the alloying additions lead to lattice shrinkage of HfB_{12} because the calculated lattice parameter of TM-doped HfB_{12} is smaller than that of the parent HfB_{12}. This result also demonstrates that these alloying elements enhance the localized hybridization between B and Hf. As a result, alloying addition effectively enhances the bond strength of B–B covalent bond and Hf–B bond. This is why the Vickers hardness of TM-doped HfB_{12} is larger than that of the HfB_{12}.

It is well known that the structural stability is related not only to the thermodynamic stability but also to the dynamic stability.[66,67] Generally, the dynamic stability of a solid is measured by the phonon frequency. The imaginary phonon frequency means the dynamic instability, and *vice versa*. To examine the dynamic stability, Fig. 4 shows the calculated phonon dispersion curves of TM-doped HfB_{12} and the HfB_{12} along the high symmetry direction. It can be seen that HfB_{12} is a dynamic stability because no imaginary phonon frequencies are found in HfB_{12}. However, we observed the imaginary phonon frequency in TM-doped HfB_{12}, indicating that TM-dopant is a dynamic instability in HfB_{12}. That is to say, these alloying additions will form the solid solution in HfB_{12}. These results are similar to the Kaner *et al.* report.[27,68]

To explore the influence of alloying elements on the thermodynamic properties of HfB_{12} superhard material, here, we consider two thermodynamic parameters: melting point and Debye temperature, respectively. Fig. 5 shows the calculated melting point of TM-doped HfB_{12} and the HfB_{12}. It can be seen that the calculated melting point of the HfB_{12} is 2093 K. In

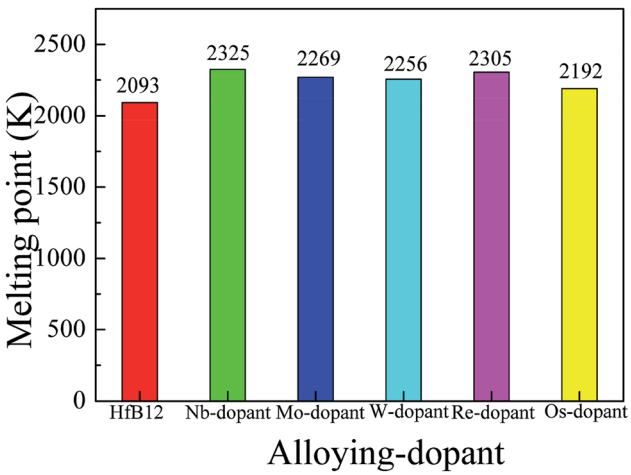

Fig. 5 Calculated melting point of TM-doped HfB_{12} and the HfB_{12}.

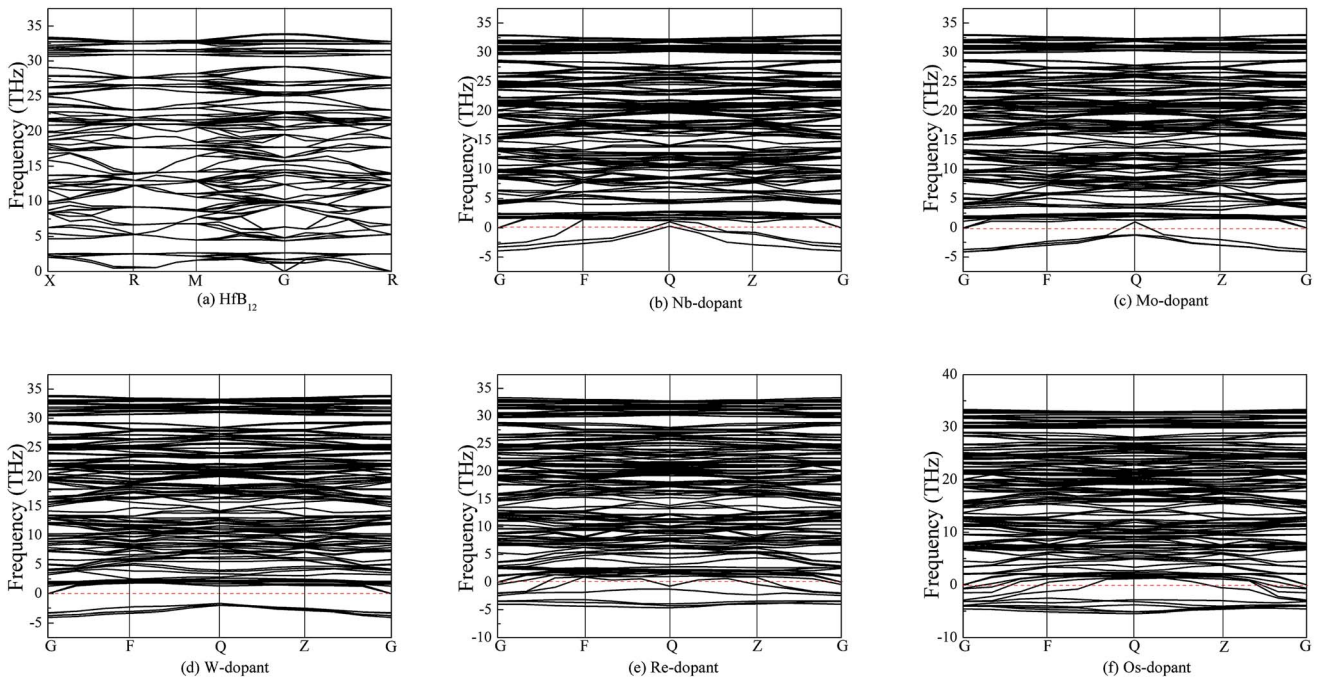

Fig. 4 . Calculated phonon dispersion curves of TM-doped HfB_{12} and the HfB_{12}, (a) the HfB_{12}, (b) Nb-dopant, (c) Mo-dopant, (d) W-dopant, (e) Re-dopant and (f) Os-dopant, respectively.

particular, we note that the calculated melting point of TM-doped HfB_{12} is much larger than that of the parent HfB_{12}. Here, the calculated melting point follows the order of Nb-dopant > Re-dopant > Mo-dopant > W-dopant > Os-dopant > HfB_{12}.

Fig. 6 shows the calculated Debye temperature of TM-doped HfB_{12} and the HfB_{12} for comparison. Here, the calculated Debye temperature of the HfB_{12} is 1010 K. Similarly, the calculated Debye temperature of TM-doped HfB_{12} is larger than that of the HfB_{12}. In our work, the trend of Debye temperature is similar to the variation of melting point. In particular, the calculated Debye temperature of Nb-doped HfB_{12} is 1102 K, which is larger than that of the other TM-doped HfB_{12} and the HfB_{12}. Therefore, we believed that these alloying elements improve the thermodynamic properties of HfB_{12}. As mentioned above, it is concluded that Nb is the best element to enhance the thermodynamic properties of HfB_{12} in comparison to the other alloying elements.

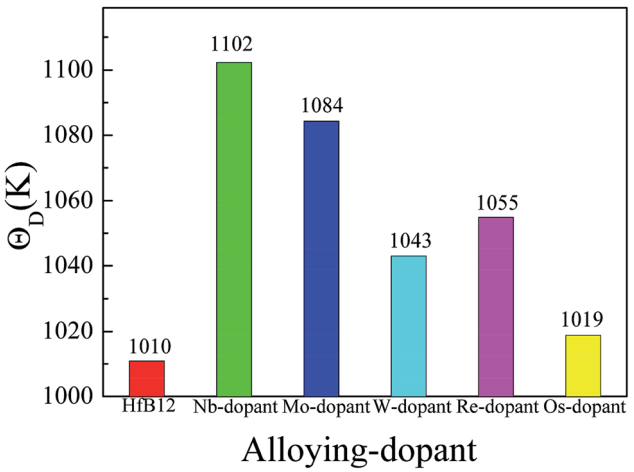

Fig. 6 Calculated Debye temperature of TM-doped HfB_{12} and the HfB_{12}.

Fig. 7 shows the calculated total and partial density of state (DOS) of TM-doped HfB_{12} and the HfB_{12}. It is found that the DOS profile of the HfB_{12} is composed of the B-2s state, B-2p state and Hf-5d state. In particular, the formation of B–B covalent bond is attributed to the localized hybridization between B and B. Based on the structural configuration, we suggest that the high hardness of HfB_{12} is attributed to the network B–B covalent bonds. The bond characteristic of B–B covalent bond is demonstrated by the charge density distribution.

When Hf atom is replaced by TM atom, it is found that the introduction of alloying element gives rise to B-2p state migration from the high energy region to the low energy region. This phenomenon will enhance the localized hybridization between B and B, and then improve the bond strength of B–B covalent bond. In addition, the band migration of B-2p state also changes the localized hybridization between Hf and B. As a result, the formation of B–B covalent bond and Hf–B bond enhances the Vickers hardness of the HfB_{12}. This result is well affirmed by the charge density distribution.

To reveal the nature of Vickers hardness, Fig. 8 displays the calculated charge density distribution in (001) plane for TM-doped HfB_{12} and the HfB_{12}. For charge density distribution, the red color means the maximum localization of electrons and

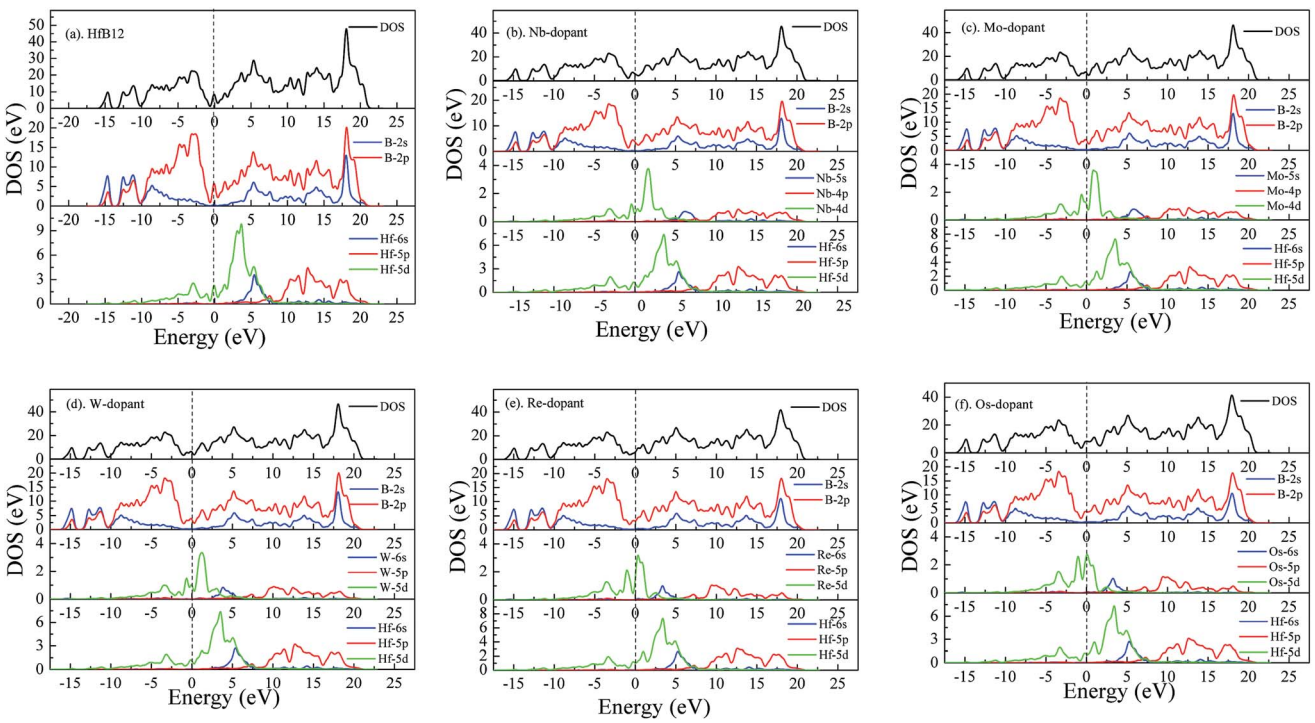

Fig. 7 Calculated density of state of TM-doped HfB_{12} and the HfB_{12}, (a) the HfB_{12}, (b) Nb-dopant, (c) Mo-dopant, (d) W-dopant, (e) Re-dopant and (f) Os-dopant, respectively.

the blue color implies the maximum delocalization of electrons.[69] Compared to the other alloying elements, it can be seen that the alloying element of Re markedly improves the Vickers hardness of the HfB_{12}. Hence, we will focus on the charge density distribution between HfB_{12} and Re-doped HfB_{12}.

From Fig. 8, firstly, we observe the formation of directional B–B covalent bonds because of the strong localized hybridization between B and Hf. The B icosahedrons cage will form two different B–B covalent bonds, which are the origin of high hardness. For the parent HfB_{12}(see Fig. 8(a)), in our work, the calculated bond length of B–B covalent bond is 1.679 Å and 1.773 Å, respectively, which are in good agreement with the other theoretical result (1.682 Å).[65] In addition we find that the calculated bond length of Hf–B bond is 2.744 Å. In particular, the B–B covalent bonds will form the 3D-network bond, which can improve the mechanical properties of HfB_{12}. Therefore, it is concluded that the Vickers hardness of HfB_{12} is also affected by the bond strength of Hf–B bond in addition to the B–B covalent bonds.

However, we find that the introduction of alloying element can improve the localize hybridization between B and the near B, which is demonstrated by the bond length of B–B covalent bond. From Fig. 8, it can be seen that the bond length of B–B covalent bond of TM-doped HfB_{12}(near TM atom) is shorter

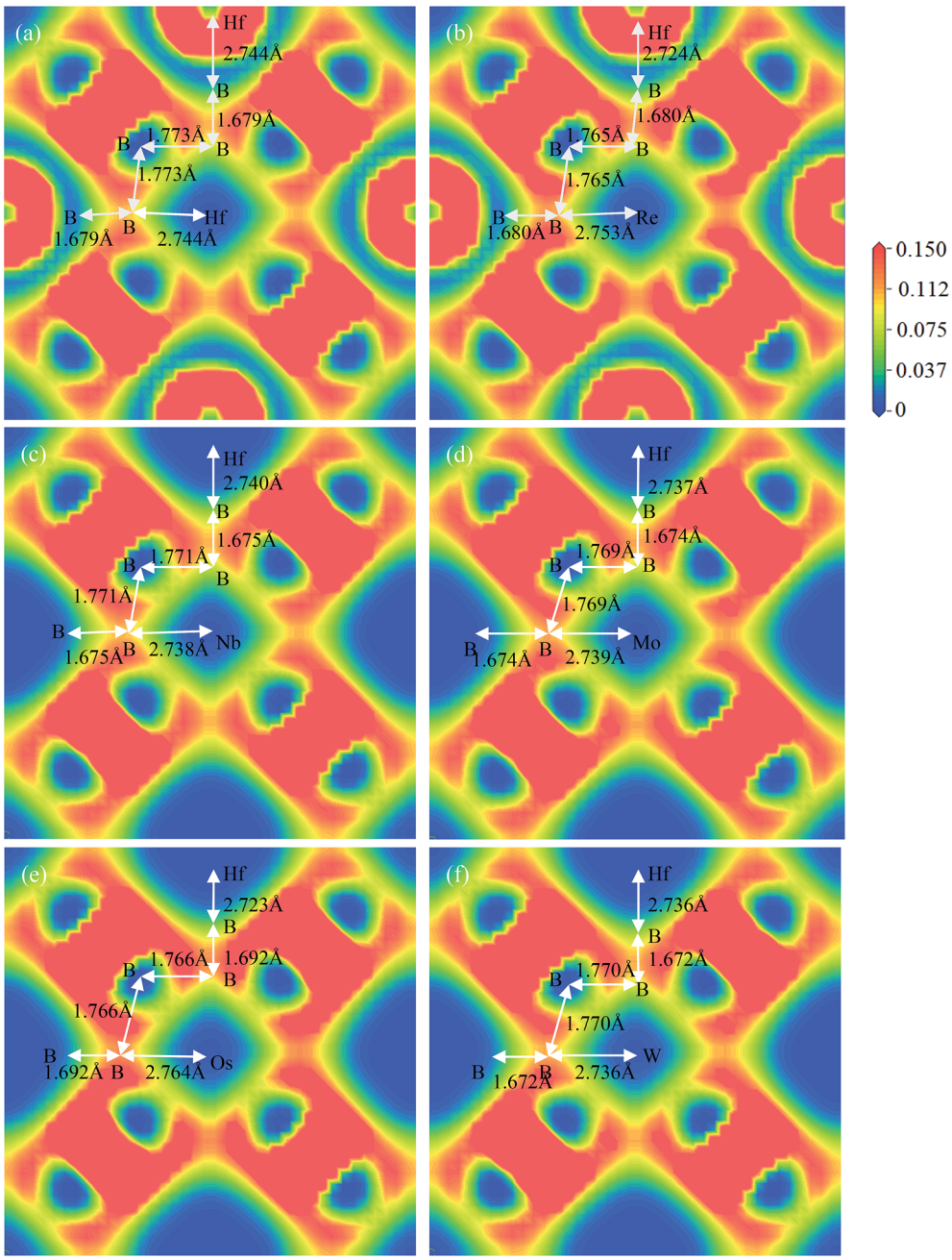

Fig. 8 Calculated charge density distribution along the (001) plane, (a) the HfB_{12}, (b) Re-dopant, (c) Nb-dopant, (d) Mo-dopant, (e) Os-dopant and (f) W-dopant, respectively.

than that of the corresponding B–B covalent bond of HfB_{12}(1.773 Å). On the other hand, it is find that the calculated bond length of Hf–B bond for TM-doped HfB_{12} is also shorter than that of the corresponding Hf–B bond for HfB_{12}. Namely, the alloying addition can improve the electronic interaction between Hf and B atoms. This is why the Vickers hardness of TM-doped HfB_{12} is larger than that of the HfB_{12}.

For example, we find that the introduction of alloying element (Re) improves the localized hybridization between B and Hf. From Fig. 7 and 8, the introduction of alloying element (Re) changes the charge interaction between B and Hf, and then improves the bonding state. Here, the calculated bond length of the corresponding B–B covalent bond is 1.680 Å along the *a*–*c* plane and 1.765 Å along the shear direction, respectively. There is well explained why the shear deformation resistance of TM-doped HfB_{12} is stronger than that of the parent HfB_{12}. On the other hand, the calculated bond length of Hf–B bond is 2.724 Å, which is shorter than the corresponding Hf–B bond for the HfB_{12}. As mentioned above, it is concluded that alloying is an effective method to improve the Vickers hardness of TMBs superhard material.

4. Conclusions

In summary, we apply the first-principles calculations to investigate the improvement of Vickers hardness, melting point and Debye temperature of HfB_{12} with alloying element, together with the HfB_{12} for comparison. We consider five transition metals: Nb(4d-), Mo(4d-), W(5d-), Re(5d-) and Os(5d-) respectively. The results show that the calculated Vickers hardness of HfB_{12} is 39.3 GPa, which is in good agreement with the other theoretical result. In particular, the calculated Vickers hardness of TM-doped HfB_{12} is bigger than 40 GPa, indicating that TM-doped HfB_{12} is a novel superhard material. The calculated Vickers hardness of Re-doped HfB_{12} is up to 47.6 GPa, which is 21.1% larger than that of the HfB_{12}.

The variation of Vickers hardness is demonstrated by the elastic modulus and brittleness. The calculated shear modulus and Young's modulus of TM-doped HfB_{12} are larger than that of the HfB_{12}. Interestingly, the calculated shear modulus and Young's modulus of Nb(4d)-doped HfB_{12} are bigger than that of the Re(5d)-doped HfB_{12}. The calculated B/G ratio of TM-doped HfB_{12} is smaller than that of the HfB_{12}, indirectly demonstrates that the Vickers hardness of TM-doped HfB_{12} is bigger than that of the HfB_{12}. In addition, the calculated melting point and Debye temperature of TM-doped HfB_{12} are larger than that of the HfB_{12}. In particular, the calculated melting point and Debye temperature of Nb-doped HfB_{12} are 2325 K and 1102 K, which are higher than that of the other TM-doped HfB_{12}. The improvement of Vickers hardness is that the introduction of alloying element improves the localized hybridization between B and Hf, and then enhances the bond strength of B–B bond and Hf–B bond.

Conflicts of interest

There are no conflicts to declare.

Acknowledgements

This work is supported by grants from the National Natural Science Foundation of China (No. 51274170) and State Key Laboratory of Advanced Technology for Comprehensive Utilization of Platinum Metals (grant no. SKL-SPM-201816). We acknowledge the discussion from Lady Yun Zheng and Runxi Pan.

References

1 P. R. Jothi, K. Yubuta and B. P. T. Fokwa, *Adv. Mater.*, 2018, **30**, 1704181.
2 Y. Pan and Y. Lin, *J. Phys. Chem. C*, 2015, **119**, 23175–23183.
3 S. Ma, K. Bao, Q. Tao, C. Xu, X. Feng, X. Zhao, Y. Ge, P. Zhu and T. Cui, *Phys. Chem. Chem. Phys.*, 2019, **21**, 2697–2705.
4 Y. Pan, W. M. Guan and Y. Q. Li, *Phys. Chem. Chem. Phys.*, 2018, **20**, 15863–15870.
5 P. J. Robinson, G. Liu, S. Ciborowski, C. M. Martinez, J. R. Chamorro, X. Zhang, T. M. Mcqueen, K. H. Bowen and A. N. Alexandroca, *Chem. Mater.*, 2017, **29**, 9892–9896.
6 Y. Pan, S. Wang, X. Zhang and L. Jia, *Ceram. Int.*, 2018, **44**, 1744–1750.
7 C. Zhao, Y. Duan, J. Gao, W. Liu, H. Dong, H. Dong, D. Zhang and A. R. Oganov, *Phys. Chem. Chem. Phys.*, 2018, **20**, 24665–24670.
8 Y. Pan and B. Zhou, *Ceram. Int.*, 2017, **43**, 8763–8768.
9 A. G. Kvashnin, H. A. Zakaryan, C. Zhao, Y. Duan, Y. A. Kvashnina, C. Xie, H. Dong and A. R. Oganov, *J. Phys. Chem. Lett.*, 2018, **9**, 3470–3477.
10 Y. Pan and W. M. Guan, *Phys. Chem. Chem. Phys.*, 2017, **19**, 19427–19433.
11 P. Wang, Z. Y. Gong, J. Hu, J. Pu and W. J. Cao, *Surf. Eng.*, 2019, **35**, 627–634.
12 Y. Pan, P. Mao, H. Jiang, Y. Wan and W. Guan, *Ceram. Int.*, 2017, **43**, 5274–5282.
13 P. Wang, T. Wu, Y. T. Xiao, L. Zhang, J. Pu, W. J. Cao and X. M. ZHong, *Vacuum*, 2017, **142**, 21–28.
14 Y. Pan and C. Jing, *Ceram. Int.*, 2019, **45**, 21373–21378.
15 G. Akopov, M. T. Yeung and R. B. Kaner, *Adv. Mater.*, 2017, **29**, 1604506.
16 Y. Pan, Y. Lin and C. Tong, *J. Phys. Chem. C*, 2016, **120**, 21762–21769.
17 L. H. Huang, Y. R. Zhao, G. T. Zhang, M. G. Zhang, P. Y. Li and Y. F. Hu, *Mol. Phys.*, 2019, **117**, 547–556.
18 G. Zhang, R. Gao, Y. Zhao, T. Bai and Y. Hu, *J. Alloys Compd.*, 2017, **723**, 802–810.
19 G. Zhang, T. Bai, Y. Zhao and Y. Hu, *Materials*, 2016, **9**, 703.
20 Y. Pan, X. Wang, S. Li, Y. Li and M. Wen, *RSC Adv.*, 2018, **8**, 18008–18015.
21 X. Li, Y. Tao and F. Peng, *J. Alloys Compd.*, 2016, **687**, 579–585.
22 Z. Q. Chen, Y. S. Peng, M. Hu, C. M. Li and Y. T. Luo, *Ceram. Int.*, 2016, **42**, 6624–6631.
23 Y. Pan and Y. Lin, *JOM*, 2017, **69**, 2009–2013.
24 R. Mohammadi, C. L. Turner, M. Xie, M. T. Yeung, A. T. Lech, S. H. Tolbert and R. B. Kaner, *Chem. Mater.*, 2016, **28**, 632–637.

25 P. Wang, T. Wu, Y. T. Xiao, J. Pu, X. Y. Guo, J. Huang and C. L. Xiang, *J. Mater. Eng. Perform.*, 2016, **25**, 3972–3976.
26 P. Wang, T. Wu, Y. T. Xiao, J. Pu and X. Y. Guo, *Mater. Lett.*, 2016, **182**, 27–31.
27 G. Akopov, M. T. Yeung, C. L. Turner, R. Mohammadi and R. B. Kaner, *J. Am. Chem. Soc.*, 2016, **138**, 5714–5721.
28 M. T. Yeung, J. Lei, R. Mohammadi, C. L. Turner, Y. Wang, S. H. Tolbert and R. B. Kaner, *Adv. Mater.*, 2016, **28**, 6993–6998.
29 G. Akopov, M. T. Yeung, Z. C. Sobell, C. L. Turner, C. W. Lin and R. B. Kaner, *Chem. Mater.*, 2016, **28**, 6605–6612.
30 A. G. V. D. Geest and A. N. Kolmogorov, *Calphad*, 2014, **46**, 184–204.
31 G. Akopov, I. Roh, Z. C. Sobell, M. T. Yeung and R. B. Kaner, *Dalton Trans.*, 2018, **47**, 6683–6691.
32 Y. Liang, Y. Zhang, H. Jiang, L. Wu, W. Zhang, K. Heckenberger, K. Hofmann, A. Reitz, F. C. Stober and B. Albert, *Chem. Mater.*, 2019, **31**, 1075–1083.
33 A. Latini, L. V. Rau, D. Ferro, R. Teghil, V. R. Albertini and S. Barinov, *Chem. Mater.*, 2008, **20**, 4507–4511.
34 N. H. Miao, B. S. Sa, J. Zhou and Z. M. Sun, *Comput. Mater. Sci.*, 2011, **50**, 1559–1566.
35 Y. Pan, P. Wang and C. Zhang, *Ceram. Int.*, 2018, **44**, 12357–12362.
36 D. Li, X. Zhang, J. Li, L. Zhao, F. Wang and X. Chen, *Vacuum*, 2019, **169**, 108883.
37 Y. Pan, *Mater. Res. Bull.*, 2017, **93**, 56–62.
38 S. Wang, Y. Pan, Y. Lin and C. Tong, *Comput. Mater. Sci.*, 2018, **146**, 18–25.
39 Y. Pan, S.-L. Wang and C.-M. Zhang, *Vacuum*, 2018, **151**, 205–208.
40 W. Ping, W. Ting, P. Hao and G. X. Yang, *Mater. Lett.*, 2016, **170**, 171–174.
41 Y. Pan and C. Jin, *Vacuum*, 2017, **143**, 165–168.
42 R. Hill, *Proc. Phys. Soc. A.*, 1952, **65**, 349.
43 Y. Pan and M. Wen, *Thin Solid Films*, 2018, **664**, 46–51.
44 S. F. Pugh, *Philos. Mag. A*, 1954, **45**, 823–843.
45 Y. Pan, Y. Li and Q. Zheng, *J. Alloys Compd.*, 2019, **789**, 860–866.
46 S. Zhu, X. Zhang, J. Chen, C. Liu, D. Li, H. Yu and F. Wang, *Vacuum*, 2019, **165**, 118–126.
47 Y. Pan, C. Jing and Y. P. Wu, *Vacuum*, 2019, **167**, 374–381.
48 Y. Pan, *J. Alloys Compd.*, 2019, **779**, 813–820.
49 H. P. Komsa and A. V. Krasheninnikov, *Phys. Rev. B: Condens. Matter Mater. Phys.*, 2015, **91**, 125304.
50 S. Cristol, J. F. Paul, E. Payen, D. Bougeard, S. Clemendot and F. Hutschka, *J. Phys. Chem. B*, 2002, **106**, 5659–5667.
51 M. Alouani and R. C. Albers, *Phys. Rev. B: Condens. Matter Mater. Phys.*, 1991, **43**, 6500–6509.
52 S. Wang and Y. Pan, *J. Am. Ceram. Soc.*, 2019, **102**, 4822–4834.
53 Y. Pan, Y. Lin, H. Wang and C. Zhang, *Mater. Des.*, 2015, **86**, 259–265.
54 D. Connétable and O. Thomas, *Phys. Rev. B: Condens. Matter Mater. Phys.*, 2009, **79**, 094101.
55 M. D. Segall, P. J. D. Lindan, M. J. Probert, C. J. Pickard, P. J. Hasnip, S. J. Clark and M. C. Payne, *J. Phys.: Condens. Matter*, 2002, **14**, 2717–2744.
56 Y. Pan, *Int. J. Hydrogen Energy*, 2018, **43**, 3087–3091.
57 J. P. Perdew, K. Burke and M. Ernzerhof, *Phys. Rev. Lett.*, 1996, **77**, 3865–3868.
58 Y. Pan, *Ceram. Int.*, 2019, **45**, 18315–18319.
59 W. A. Harrison, *Phys. Rev. B: Condens. Matter Mater. Phys.*, 1990, **41**, 6008–6019.
60 Y. Pan and M. Wen, *Int. J. Hydrogen Energy*, 2018, **43**, 22055–22063.
61 Y. Pan and W. M. Guan, *Ceram. Int.*, 2018, **44**, 9893–9898.
62 X. Bi, X. Hu and Q. Li, *Results Phys.*, 2019, **15**, 102607.
63 Y. Pan, *Int. J. Hydrogen Energy*, 2019, **44**, 18153–18158.
64 N. Korozlu, K. Colakoglu, E. Deligoz and S. Aydin, *J. Alloys Compd.*, 2013, **546**, 157–164.
65 H. Werheit, V. Filipov, K. Shirai, H. Dekura, N. Shitsevalova, U. Schwarz and M. Armbruster, *J. Phys.: Condens. Matter*, 2011, **23**, 065403.
66 Y. Pan, Y. Q. Li, Q. H. Zheng and Y. Xu, *J. Alloys Compd.*, 2019, **786**, 621–626.
67 Y. Pan and W. M. Guan, *Inorg. Chem.*, 2018, **57**, 6617–6623.
68 G. Akopov, M. T. Yeung, C. L. Turner, R. L. Li and R. B. Kaner, *Inorg. Chem.*, 2016, **55**, 5051–5055.
69 Y. Pan and W. Guan, *J. Power Sources*, 2016, **325**, 246–251.